

Nonmesonic Quantum Many-Body Scars in a 1D Lattice Gauge Theory

Zi-Yong Ge,^{1,*} Yu-Ran Zhang,^{2,†} and Franco Nori^{1,3,4,‡}

¹Theoretical Quantum Physics Laboratory, Cluster for Pioneering Research, RIKEN, Wako-shi, Saitama 351-0198, Japan

²School of Physics and Optoelectronics, South China University of Technology, Guangzhou 510640, China

³Quantum Information Physics Theory Research Team,

Center for Quantum Computing, RIKEN, Wako-shi, Saitama 351-0198, Japan

⁴Department of Physics, University of Michigan, Ann Arbor, Michigan 48109-1040, USA

We investigate the meson excitations (particle-antiparticle bound states) in quantum many-body scars of a 1D \mathbb{Z}_2 lattice gauge theory coupled to a dynamical spin- $\frac{1}{2}$ chain as a matter field. By introducing a string representation of the physical Hilbert space, we express a scar state $|\Psi_{n,l}\rangle$ as a superposition of all string bases with an identical string number n and a total length l . For the small- l scar state $|\Psi_{n,l}\rangle$, the gauge-invariant spin exchange correlation function of the matter field hosts an exponential decay as the distance increases, indicating the existence of stable mesons. However, for large l , the correlation function exhibits a power-law decay, signaling the emergence of nonmesonic excitations. Furthermore, we show that this mesonic-nonmesonic crossover can be detected by the quench dynamics, starting from two low-entangled initial states, respectively, which are experimentally feasible in quantum simulators. Our results expand the physics of quantum many-body scars in lattice gauge theories and reveal that the nonmesonic state can also manifest ergodicity breaking.

Introduction.—Because of the development of quantum simulations [1–8], out-of-equilibrium quantum many-body physics has been attracting growing interests [9]. The Eigenstate Thermalization Hypothesis (ETH) postulates that generic isolated nonintegrable quantum many-body systems exhibit ergodicity [10–14], and thus, the unitary quantum evolution of the systems can result in an equilibrium state described by statistical mechanics. Though ETH was thought to be general, there are several counterexamples, e.g., quantum integrable systems [15, 16] and many-body localizations [17–23]. These two examples are called strong ergodicity breaking, since most of the eigenstates violate the ETH. Recent experimental and theoretical works demonstrate that there exists a new type of ETH-violating eigenstates in some specific nonintegrable quantum many-body systems, dubbed quantum many-body scar (QMBS) states [24–44]. Generally, the number of QMBS states is exponentially smaller than the Hilbert space dimension, so they can be considered as weak ergodicity breaking. One typical class of QMBS states is constructed by spectrum-generated algebras [37, 38, 43, 45], whose eigenenergies are equally spaced, dubbed towers of QMBSs [43]. Thus, if the initial state is a superposition of these scar states, there will exist a perfect revival dynamics indicating the ETH violation.

Empirically, kinetically constrained systems are thought more likely to host QMBSs. Thus, as a typical instance, lattice gauge theories (LGTs) [46–62] have attracted considerable interest to study QMBSs [63–70]. Meanwhile, quasiparticles are significant for understanding the towers of QMBSs [71]. In LGTs, particles can be pairwise confined into mesons, which are one of the most important quasiparticles, closely related to the towers of QMBS [63–66, 72, 73]. For instance, the scar dynamics in the PXP model [65] can be understood as the string inversion of a $U(1)$ LGT, where a particle and an antiparticle form a bound state, a stable meson. Therefore, one natural question is whether stable mesons are necessary conditions for the towers of QMBSs in LGTs. A recent

work [36] reports a special type of QMBSs in a spin chain with conserved domain wall (equivalent to a \mathbb{Z}_2 LGT), which is generated by nonlocal operators. Based on these QMBSs, we address the above questions, and further reveal more non-trivial physics when investigating QMBSs in LGTs.

In this Letter, we study this type of QMBSs in a \mathbb{Z}_2 LGT and demonstrate that it can manifest both *mesonic* and *non-mesonic* features. First, we introduce a string representation to describe the physical Hilbert space in a specific gauge sector. In this representation, the exact wave function of the QMBS state $|\Psi_{n,l}\rangle$ is written as an equal superposition of all string bases with an identical string number n and a total string length l . We identify the meson properties in $|\Psi_{n,l}\rangle$ by calculating the gauge-invariant spin exchange correlation function of the matter field. Our results show that there exist stable mesons for small l , while the quasiparticles are non-mesonic for large l . Moreover, we propose a feasible approach to demonstrate the mesonic-nonmesonic crossover with quantum simulators, by observing the quench dynamics of the system initially at two different low-entangled states, respectively.

Model.—Here, we consider a 1D \mathbb{Z}_2 LGT minimally coupled to a dynamical spin- $\frac{1}{2}$ chain as a matter field. The Hamiltonian has a form $\hat{H} = \hat{H}_K + H_E + \hat{H}_\mu$, with

$$\begin{aligned}\hat{H}_K &= -J \sum_{j=1}^L (\hat{\sigma}_j^+ \hat{\tau}_{j+\frac{1}{2}}^z \hat{\sigma}_{j+1}^- + \text{H.c.}), \\ \hat{H}_E &= -h \sum_{j=1}^L \hat{\tau}_{j+\frac{1}{2}}^x, \quad \hat{H}_\mu = \mu \sum_{j=1}^L \hat{\sigma}_j^+ \hat{\sigma}_j^-, \end{aligned} \quad (1)$$

where $\hat{\sigma}_j^\alpha$ and $\hat{\tau}_{j+\frac{1}{2}}^\alpha$ are both Pauli matrices describing the matter and gauge fields, respectively, and L is the system size. The matter field lives on the site, while the gauge field is on the link. The kinetic term \hat{H}_K describes the minimal gauge-matter coupling with strength J , the second term \hat{H}_E describes an electric field with strength h , and the last term \hat{H}_μ denotes the potential of the matter field. We consider peri-

odic boundary conditions, i.e., $\hat{\sigma}_1^\alpha = \hat{\sigma}_{L+1}^\alpha$ and $\hat{\tau}_{1+\frac{1}{2}}^\alpha = \hat{\tau}_{L+1+\frac{1}{2}}^\alpha$. The Hamiltonian \hat{H} is \mathbb{Z}_2 gauge invariant with a generator $\hat{G}_j = \hat{\tau}_{j-\frac{1}{2}}^x \hat{\sigma}_j^z \hat{\tau}_{j+\frac{1}{2}}^x$. In addition to the gauge structure, there also exists the spin $U(1)$ symmetry in \hat{H} , where the total spin charge $\sum_{j=1}^L \hat{\sigma}_j^+ \hat{\sigma}_j^-$ is conserved. Note that this \mathbb{Z}_2 LGT can be experimentally addressed in various quantum simulators [74–81].

Without loss of generality, we fix the system to the gauge sector $\hat{G}_j = 1$, with an even number of total spin charges for each physical basis. With a dual transformation, the original Hamiltonian \hat{H} can be mapped to a local spin chain [82]

$$\begin{aligned} \hat{H}_K &= -\frac{J}{2} \sum_j (\hat{Z}_{j+\frac{1}{2}} - \hat{X}_{j-\frac{1}{2}} \hat{Z}_{j+\frac{1}{2}} \hat{X}_{j+\frac{3}{2}}), \\ \hat{H}_E &= -h \sum_j \hat{X}_{j+\frac{1}{2}}, \quad \hat{H}_\mu = \frac{\mu}{2} \sum_j (1 - \hat{X}_{j-\frac{1}{2}} \hat{X}_{j+\frac{1}{2}}), \end{aligned} \quad (2)$$

where $\hat{X}_{j+\frac{1}{2}} = \hat{\tau}_{j+\frac{1}{2}}^x$ and $\hat{Z}_{j+\frac{1}{2}} = \hat{\sigma}_j^x \hat{\tau}_{j+\frac{1}{2}}^z \hat{\sigma}_{j+1}^x$ are also Pauli matrices.

Figure 1(a) plots the half-chain von Neumann entropies, $S = \text{Tr} \hat{\rho}_{L/2} \ln \hat{\rho}_{L/2}$, of the whole eigenstates in the half-filling case ($\sum_{j=1}^L \hat{\sigma}_j^+ \hat{\sigma}_j^- = L/2$), where $\hat{\rho}_{L/2}$ is the half-chain density matrix. The entanglement entropies of states near the middle of the spectrum approach the value for a random state $S^{\text{ran}} = (L \ln 2 - 1)/2$ [83], which demonstrates that most of the eigenstates obey ETH.

As shown in Ref. [36], a pyramid-like structure of scar states exists for the dual Hamiltonian (2), see Figs. 1(a,b). These scar states cannot be generated by local operators and are very distinct from the conventional towers of QMBSs. However, they have not been fully investigated. Specifically, it is still unclear whether stable meson excitations dominate the scar dynamics, like most of conventional QMBSs in LGTs. In addition, an experimental proposal to detect these QMBSs from the nontrivial quench dynamics in quantum simulators is also a relevant issue. Hereafter, we investigate the QMBSs of \hat{H} from the viewpoint of LGTs, and uncover whether these can be described by mesonic physics. Note that while analytical discussions are based on the original Hamiltonian Eq. (1), the numerical results are obtained from the Hamiltonian (2) by exact diagonalization.

String representation.—We introduce string bases in the $\hat{G}_j = 1$ sector, which are convenient for discussing meson excitations. Because of gauge invariance, the physical Hilbert space in the fixed gauge sector can be represented by open strings. The vacuum state of string excitations can be defined as $|\Omega\rangle := |\downarrow\downarrow \dots \downarrow\downarrow\rangle \otimes |+\dots+\rangle$, where $|\downarrow\downarrow \dots \downarrow\downarrow\rangle$ is a ferromagnetic state of matter fields, and $|\tau\rangle = |+\dots+\rangle$ is the state of gauge fields with all links being polarized at $\hat{\tau}^x = 1$. A state with one string excitation can be written as

$$|\mathcal{S}_{k,\ell}\rangle := \hat{S}_{k,\ell}^\dagger |\Omega\rangle = \hat{\sigma}_k^+ \left(\prod_{k \leq j < k+\ell} \hat{\tau}_{j+\frac{1}{2}}^M \right) \hat{\sigma}_{k+\ell}^+ |\Omega\rangle, \quad (3)$$

where $\hat{\tau}_{j+\frac{1}{2}}^M = |-\rangle\langle+|$, and k denotes the string position, and ℓ denotes the string length. Note that, if the operator $\hat{S}_{k,\ell}^\dagger$ is

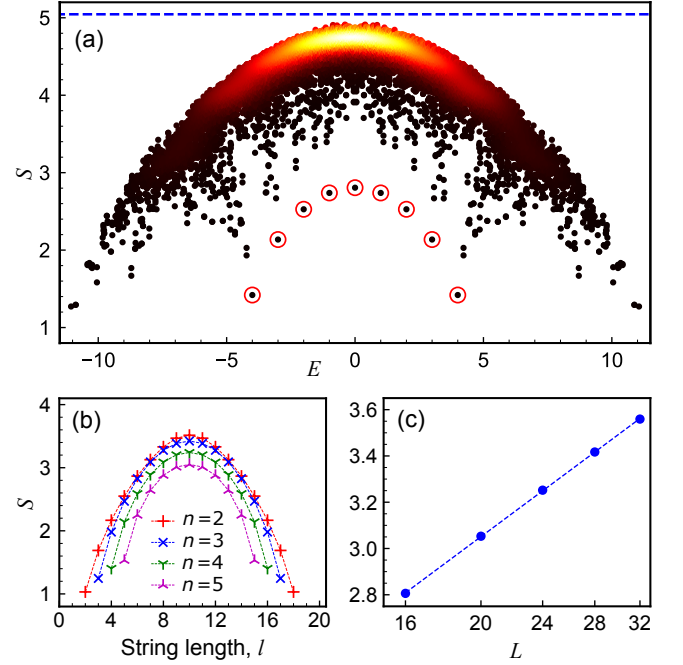


FIG. 1. Half-chain von Neumann entropy S . (a) The distribution of S for all eigenstates of Hamiltonian (1) in the half-filling sector (i.e., string number $n = L/4$) with $L = 16, J = 1, h = 0.5$. The color codes the density of states (warmer colors imply higher density). The blue dashed line represents the entanglement entropy of the random state $S^{\text{ran}} = (L \ln 2 - 1)/2 \approx 5.05$. The data points in red circles correspond to the eigenstates in Eq. (5). (b) Pyramidlike structure of $|\Psi_{n,l}\rangle$ for $L = 20$. Different colors represent different numbers of strings n . (c) The size scaling of the entanglement entropy for the QMBS state $|\Psi_{L/4, L/2}\rangle$. The dashed line shows linear fitting: $S \sim \ln L$.

local [i.e., $\ell \sim O(1)$], the corresponding string excitation can be regarded as a meson.

An arbitrary gauge invariant basis can be written as

$$|\{\mathcal{S}_{k_j, \ell_j}\}_n^l\rangle = \hat{S}_{k_1, \ell_1}^\dagger \hat{S}_{k_2, \ell_2}^\dagger \dots \hat{S}_{k_{n-1}, \ell_{n-1}}^\dagger \hat{S}_{k_n, \ell_n}^\dagger |\Omega\rangle, \quad (4)$$

where $k_j > k_i + \ell_i$, for $j > i$, n is the number of strings and equals half of total spin charges, $l := \sum_{j=1}^n \ell_j$ is the total string length, and the parity is defined as $P_{\{\mathcal{S}_{k_j, \ell_j}\}_n^l} = \exp(-i\pi \sum_{j=1}^n k_j)$. While l determines the energy of the electric-field term $\hat{H}_E |\{\mathcal{S}_{k_j, \ell_j}\}_n^l\rangle = h(2l - L) |\{\mathcal{S}_{k_j, \ell_j}\}_n^l\rangle$, n determines the energy of the potential term $\hat{H}_\mu |\{\mathcal{S}_{k_j, \ell_j}\}_n^l\rangle = 2\mu n |\{\mathcal{S}_{k_j, \ell_j}\}_n^l\rangle$.

Exact quantum many-body scars.—We introduce the pyramidlike QMBS states in this \mathbb{Z}_2 LGT [36], whose wave functions in the string representation are written as

$$|\Psi_{n,l}\rangle = \mathcal{N}_{n,l} \sum_{\{k_j, \ell_j\}} P_{\{\mathcal{S}_{k_j, \ell_j}\}_n^l} |\{\mathcal{S}_{k_j, \ell_j}\}_n^l\rangle, \quad (5)$$

where $\mathcal{N}_{n,l}$ is a normalization factor. That is, $|\Psi_{n,l}\rangle$ is an equal superposition of all string bases with both the same string number n and total length l , and the phase is determined by the parity of each basis. Since $0 < \ell_j < L$, the

quantum numbers n and l satisfy $n \leq l \leq L-n$. Thus, there are $(L-2n+1)$ of eigenstates in the sector with $\sum_{j=1}^L \hat{\sigma}_j^+ \hat{\sigma}_j^- = 2n$ total spin charge. It can be proved that $\hat{H}_K |\Psi_{n,l}\rangle = 0$ [see more details in Supplemental Material (SM) [84]], and the eigenenergy of $|\Psi_{n,l}\rangle$ is $\varepsilon_{n,l} = 2hl + 2\mu n - hL$, which can be away from edges of the spectrum corresponding to a high-energy eigenstate, see Fig. 1(a). In addition, the scar states $|\Psi_{n,l}\rangle$ host the sub-volume-law entanglement entropy, i.e., $S \sim \ln L$, demonstrating the ETH violation, see Fig. 1(c).

The scar state $|\Psi_{n,l}\rangle$ can also be expressed in terms of generating operators. First, we consider a simple case $|\Psi_{n,n}\rangle$, which only contains n length-1 string excitation. We can construct a ladder operator [66] $\hat{S}^\dagger := \sum_j P_{S_{j,1}} \hat{S}_{j,1}^\dagger$, and the eigenstate $|\Psi_{n,n}\rangle$ can be obtained as

$$|\Psi_{n,n}\rangle = \mathcal{A}_n (\hat{S}^\dagger)^n |\Omega\rangle, \quad (6)$$

where \mathcal{A}_n is a normalization factor. Then, we introduce another operator [36] $\hat{L}_m^\dagger = \sum_j (\sum_{k \leq m} \prod_{\ell \leq k} \hat{P}_{j+\frac{1}{2}-\ell}^-) \hat{\sigma}_j^- \hat{\tau}_{j+\frac{1}{2}}^M \hat{\sigma}_{j+1}^+$, where $\hat{P}^- := |- \rangle \langle -|$. The action of \hat{L}_m^\dagger is to enlarge the total string length by 1 without changing the parity. Using \hat{L}_m^\dagger , we obtain the eigenstate $|\Psi_{n,n+m}\rangle$ as [36, 84]

$$|\Psi_{n,n+m}\rangle = \mathcal{D}_{n,m} \hat{L}_m^\dagger |\Psi_{n,n+m-1}\rangle \quad (7)$$

where $\mathcal{D}_{n,m}$ is a normalization factor. Equations (6, 7) indicate that the scar state $|\Psi_{n,n}\rangle$, like the conventional tower of QMBSs, is generated by *local* operators, while $|\Psi_{n,n+m}\rangle$ is generated by *nonlocal* operators. Thus, intuitively, as the total string length l increases, the meson properties for the scar state $|\Psi_{n,l}\rangle$ are expected to be significantly changed.

Mesonic-nonmesonic crossover.—Mesons, as a type of particle-antiparticle bound states, play an important role in the dynamics of LGTs. If the system is in a confined phase, the low-energy excitation is described by mesons. In addition, in a high-energy regime, meson dynamics also closely relate to the ETH. Previous works have shown that almost all of the towers of QMBSs in LGTs originate from meson excitations [63–66, 72, 73]. For the Hamiltonian (1), the σ -spin is confined in the ground state with an arbitrary finite h [82], where the low-energy excitation is a meson. However, it is still unclear whether mesons can describe the high-energy dynamics, especially the scar dynamics.

According to Eq. (4), the σ -spin charges appear pairwise forming string excitations. For small l , e.g., $|\Psi_{n,n}\rangle$, two σ -spin charges are always bonded together on two nearest-neighbor sites, i.e., there only exist *local* string excitations (mesons). This suggests that these scar states should be described by stable mesons. However, as l increases, the distance between two σ spin charges of a string excitation becomes large, and *nonlocal* string excitations can emerge. Hence, intuitively, isolated σ -spin charges are expected to exist in this case, i.e., nonmesonic quasiparticles emerge. In Fig. 2(a), we present the expectation value of the electric field, defined as $\hat{M}_x := \sum_{j=1}^L \hat{\tau}_{j+\frac{1}{2}}^x$. It shows that $\langle \hat{M}_x \rangle$ of small- l scar states are located at the edge of the spectrum, which

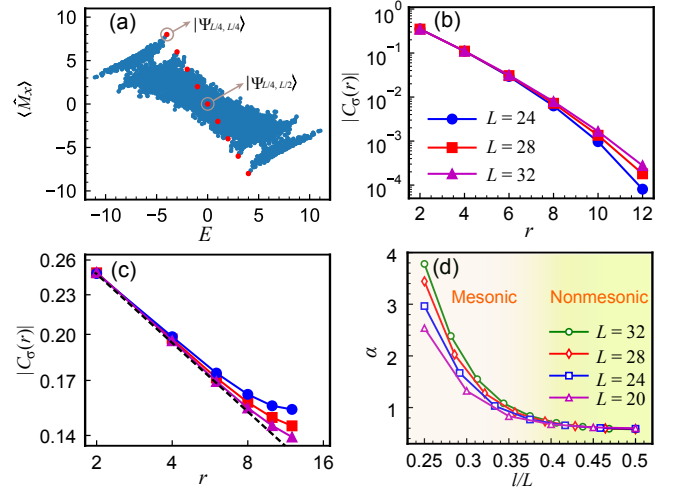


FIG. 2. Properties of mesons. (a) Expectation values of the electric field for all eigenstates at half filling with $L = 16$ and $h = 0.5$. The red dots correspond to scar states. (b,c) Gauge-invariant spin exchange correlation function of the matter field $C_\sigma(r)$ defined in Eq. (8) for $l = L/4$ and $l = L/2$, respectively. The total string number is $n = L/4$. The black dashed line is for the fit: $|C_\sigma(r)| \sim r^{-\Delta}$, with $\Delta \approx 0.35$. (d) Ratio α in Eq. (9) versus l/L for the scar state $|\Psi_{n,l}\rangle$ with $n = L/4$.

is similar to the confinement-induced non-thermal states in Refs. [63, 64]. This suggests that these scar states can be described by stable mesons. However, for large- l scar states, $\langle \hat{M}_x \rangle$ is located in the main spectrum, implying nonmesonic features. Note that we only need to consider the total string length $l \leq L/2$, and the large total string length means that l is $\approx L/2$ [85].

To further verify the above picture, we perform numerical simulations by calculating the gauge-invariant spin exchange correlation function versus the distance r [82]

$$C_\sigma(r) := \langle \Psi_{n,l} | [\hat{\sigma}_j^+ (\prod_{j \leq k < j+r} \hat{\tau}_{k+\frac{1}{2}}^z) \hat{\sigma}_{j+r}^- + h.c.] | \Psi_{n,l} \rangle, \quad (8)$$

which identifies elementary excitations. Here, if $C_\sigma(r)$ exhibits an exponential decay for increasing r , the isolated σ -spin charges cannot be detected. Thus, the quasiparticles should be composite particles of matter fields, i.e., mesons [82]. However, if $C_\sigma(r)$ exhibits a power-law decay or converges to a nonzero value with increasing r , an isolated σ -spin charge can be observed, and the quasiparticles are not mesons. Figure 2(b) shows that $C_\sigma(r)$ approximately exhibits an exponential decay for $|\Psi_{L/4,L/4}\rangle$, indicating that the small- l scar states are described by stable mesons. However, $C_\sigma(r)$ can exhibit a power-law decay for the state $|\Psi_{L/4,L/2}\rangle$, showing the existence of nonmesonic excitations for large l , see Fig. 2(c). Figure 2(d) plots the numerical results of the ratio

$$\alpha := -\ln C_\sigma(L/2) / \ln L. \quad (9)$$

We find that, as l/L increases, the curves of α for different system sizes gradually collapse to a single curve, show-

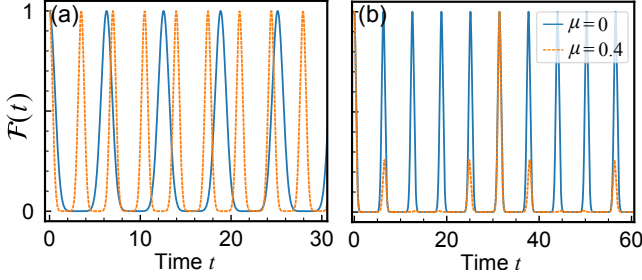


FIG. 3. Time evolution of the fidelity $\mathcal{F}(t)$ after a quantum quench for the initial states (a) $|\psi_1\rangle$ and (b) $|\psi_2\rangle$ in Eq. (10). Here, we choose $J = 1$, $h = 0.5$, and $L = 16$.

ing that $C_\sigma(r)$ gradually exhibits a power-law decay. Therefore, there exists a mesonic-nonmesonic crossover for these QMBs. Figure 2 also reveals that the stable meson excitation is not a necessary condition for the towers of QMBs in LGTs. Note that the nonmesonic excitation is a collective effect, which only emerges in many-particle systems, i.e., the filling factor n/L is finite.

Quench dynamics.—Another problem is whether the QMBS states $|\Psi_{n,l}\rangle$ can lead to nontrivial quench dynamics, which can be experimentally observed in quantum simulators. Here, we introduce two initial states

$$|\psi_1\rangle = \mathcal{B} \prod_j [1 + (-1)^j \hat{\sigma}_j^+ \hat{\tau}_{j+\frac{1}{2}}^M \hat{\sigma}_{j+1}^+] |\Omega\rangle, \quad (10a)$$

$$|\psi_2\rangle = \frac{1}{2^{L/2}} \sum_{n,l} \sum_{\{k_j, \ell_j\}} P_{\{S_{k_j, \ell_j}\}_n} |\{S_{k_j, \ell_j}\}_n\rangle, \quad (10b)$$

where \mathcal{B} is a normalization factor. Here, $|\psi_1\rangle$ is a superposition of scar states $|\Psi_{n,n}\rangle$, i.e., $|\psi_1\rangle = \sum_n \alpha_n |\Psi_{n,n}\rangle$, and $|\psi_2\rangle$ is a superposition of all scar states $|\Psi_{n,l}\rangle$, i.e., $|\psi_2\rangle = \sum_{n,l} \beta_{n,l} |\Psi_{n,l}\rangle$. It is obvious that both initial states host low entanglement entropies. Specifically, with the dual transformation in Eq. (2), $|\psi_1\rangle$ is related to the ground state of the PXP model [66], and $|\psi_2\rangle = \otimes_j |V_{2j+\frac{1}{2}, 2j+\frac{3}{2}}\rangle$, with $|V_{2j+\frac{1}{2}, 2j+\frac{3}{2}}\rangle = (|++\rangle - |+-\rangle + |-+\rangle + |--\rangle)/2$.

Figure 3 presents the fidelity $\mathcal{F}(t) := |\langle \psi_{1,2} | e^{-i\hat{H}t} | \psi_{1,2} \rangle|^2$. It shows that $\mathcal{F}(t)$ exhibits perfect revival dynamics for both initial states in Eq. (10). For the initial state $|\psi_1\rangle$, the oscillation period is $T = \pi/(h + \mu)$, see Fig. 3(a). For the initial state $|\psi_2\rangle$, if $h/\mu = p/q$, with p and q being relatively prime, the time for a perfect revival is $T = p\pi/h = q\pi/\mu$, see Fig. 3(b). The oscillation period is consistent with the eigenenergies of $|\Psi_{n,l}\rangle$. Moreover, the revival dynamics signals the ETH violation for QMBs $|\Psi_{n,l}\rangle$.

We also probe the quasiparticles during the quench dynamics. Since $|\psi_1\rangle$ is a superposition of small- l scar states, we expect a mesonic quench dynamics, i.e., mesons are always stable during the dynamics, like the scar dynamics in the PXP model [65]. For the initial state $|\psi_2\rangle$, although it is a superposition of all scar states, the large- l scar states should be dominant [84], e.g., $|\beta_{L/4, L/2}| \gg |\beta_{L/4, L/4}|$. Thus, it leads to

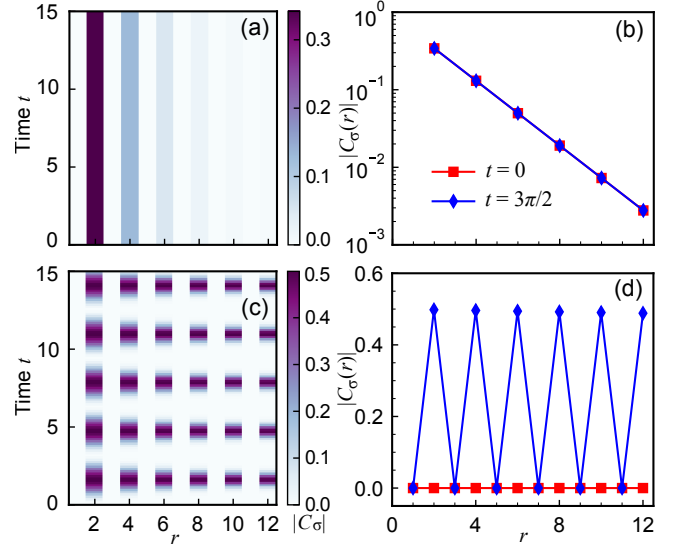


FIG. 4. Time evolution of the correlation function $C_\sigma(r)$ for two different initial states (a,b) $|\psi_1\rangle$ and (c,d) $|\psi_2\rangle$. Here, we choose $J = 1$, $h = 0.5$, $\mu = 0.4$, and $L = 24$.

nonmesonic dynamics. We calculate the gauge invariant correlation function $C_\sigma(r)$ in Eq. (8) to identify meson properties during the quench dynamics. For $|\psi_1\rangle$, we find that $C_\sigma(r)$ exhibits an exponential decay during the quench dynamics, see Figs. 4(a,b). This indicates that mesons are very stable and cannot be decomposed into isolated spin charges. However, the situation becomes different for $|\psi_2\rangle$, where $C_\sigma(r) \sim \text{const}$ for $r \rightarrow \infty$ at the specific time, see Figs. 4(c,d). Thus, the isolated spin charges dominate the dynamics, without stable mesons. Therefore, the initial states in Eq. (10) can be used to detect the mesonic-nonmesonic crossover for QMBs $|\Psi_{n,l}\rangle$ during their quench dynamics.

Experimental proposal.—The preparation of the initial states in Eq. (10) in dual systems is convenient in quantum simulators. In addition, the dual Hamiltonian (2), with three-body interactions, has also been realized with quantum gates, e.g. in superconducting circuits [79, 86]. Therefore, the mesonic-nonmesonic crossover for QMBs in this \mathbb{Z}_2 LGT can be experimentally detected with digital quantum simulations.

Summary.—We have investigated the mesons in QMBs of a \mathbb{Z}_2 LGT. By introducing the string representation, we express the wave function of each QMBS as an equal superposition of all string bases with an identical string number and total string length. We demonstrate that scar states with a small total string length are described by stable mesons, like conventional towers of QMBs in LGTs, while we find the nonmesonic excitations in the scar states with large total string length. Furthermore, this mesonic-nonmesonic crossover in QMBs can be observed from the quench dynamics with two experimentally accessible initial states. Our results bring new insights into QMBs in LGTs and reveal that the nonmesonic states can also host ergodicity breaking in LGTs, which can

be experimentally verified with quantum simulators.

Here, the mesonic-nonmesonic crossover is reminiscent of the asymptotic freedom of quarks [87, 88]. The eigenenergy of the scar state $|\Psi_{n,l}\rangle$ becomes large when increasing the total string length l . Thus, the nonmesonic excitation in large- l QMBs is in analogy with the asymptotic freedom of quarks in the high-energy regime of quantum chromodynamics. The conventional QMBs are generated by local operators, which correspond to nonfractionalized excitations [71], e.g., magnons in PXP [89] and spin-1 XY models [33], and η -pairs in Hubbard-like models [37, 38]. However, the nonmesonic excitations have some analogies with spinons [51], which are fractionalized excitations and different from conventional QMBs. Therefore, our results also reveal that nonlocal generating operators may lead to fractionalized excitations in QMBs, providing an inspiration for studying the nontrivial excitation in QMBs. Here, nonlocal generating operators are necessary for the nonmesonic QMBs, since they can separate two matter particles of a meson. However, it is still unclear which types of generating operators can induce these nontrivial physics. Another interesting issue is whether the above physics can be generalized to other gauge groups or high-dimensional LGTs [56, 90]. These open questions deserve further study.

Acknowledgments.—We thank Marcello Dalmonte, Zongping Gong, and Rui-Zhen Huang for insightful discussions and useful suggestions. This work is supported in part by: Nippon Telegraph and Telephone Corporation (NTT) Research, the Japan Science and Technology Agency (JST) [via the Quantum Leap Flagship Program (Q-LEAP), and the Moonshot R&D Grant Number JPMJMS2061], the Asian Office of Aerospace Research and Development (AOARD) (via Grant No. FA2386-20-1-4069), and the Office of Naval Research (ONR) Global (via Grant No. N62909-23-1-2074).

* ziyong.ge@riken.jp

† yuranzhang@scut.edu.cn

‡ fnori@riken.jp

- [1] M. Lewenstein, A. Sanpera, V. Ahufinger, B. Damski, A. Sen(De), and U. Sen, Ultracold atomic gases in optical lattices: mimicking condensed matter physics and beyond, *Adv. Phys.* **56**, 243 (2007).
- [2] I. Bloch, J. Dalibard, and W. Zwerger, Many-body physics with ultracold gases, *Rev. Mod. Phys.* **80**, 885 (2008).
- [3] I. Buluta and F. Nori, Quantum simulators, *Science* **326**, 108 (2009).
- [4] I. Buluta, S. Ashhab, and F. Nori, Natural and artificial atoms for quantum computation, *Rep. Prog. Phys.* **74**, 104401 (2011).
- [5] M. Dalmonte and S. Montangero, Lattice gauge theory simulations in the quantum information era, *Contemp. Phys.* **57**, 388 (2016).
- [6] I. M. Georgescu, S. Ashhab, and F. Nori, Quantum simulation, *Rev. Mod. Phys.* **86**, 153 (2014).
- [7] C. Gross and I. Bloch, Quantum simulations with ultracold atoms in optical lattices, *Science* **357**, 995 (2017).
- [8] A. Browaeys and T. Lahaye, Many-body physics with individually controlled Rydberg atoms, *Nat. Phys.* **16**, 132 (2020).
- [9] A. Polkovnikov, K. Sengupta, A. Silva, and M. Vengalattore, Colloquium: Nonequilibrium dynamics of closed interacting quantum systems, *Rev. Mod. Phys.* **83**, 863 (2011).
- [10] J. M. Deutsch, Quantum statistical mechanics in a closed system, *Phys. Rev. A* **43**, 2046 (1991).
- [11] M. Srednicki, Chaos and quantum thermalization, *Phys. Rev. E* **50**, 888 (1994).
- [12] M. Srednicki, The approach to thermal equilibrium in quantized chaotic systems, *Journal of Physics A: Mathematical and General* **32**, 1163 (1999).
- [13] M. Rigol, V. Dunjko, and M. Olshanii, Thermalization and its mechanism for generic isolated quantum systems, *Nature (London)* **452**, 854 (2008).
- [14] L. D'Alessio, Y. Kafri, A. Polkovnikov, and M. Rigol, From quantum chaos and eigenstate thermalization to statistical mechanics and thermodynamics, *Advances in Physics* **65**, 239 (2016).
- [15] T. Kinoshita, T. Wenger, and D. S. Weiss, A quantum Newton's cradle, *Nature* **440**, 900 (2006).
- [16] M. Rigol, V. Dunjko, V. Yurovsky, and M. Olshanii, Relaxation in a Completely Integrable Many-Body Quantum System: An Ab Initio Study of the Dynamics of the Highly Excited States of 1D Lattice Hard-Core Bosons, *Phys. Rev. Lett.* **98**, 050405 (2007).
- [17] D. M. Basko, I. L. Aleiner, and B. L. Altshuler, Metal-insulator transition in a weakly interacting many-electron system with localized single-particle states, *Ann. Phys.* **321** (2006).
- [18] A. Pal and D. A. Huse, Many-body localization phase transition, *Phys. Rev. B* **82**, 174411 (2010).
- [19] J. A. Kjäll, J. H. Bardarson, and F. Pollmann, Many-Body Localization in a Disordered Quantum Ising Chain, *Phys. Rev. Lett.* **113**, 107204 (2014).
- [20] D. A. Huse, R. Nandkishore, and V. Oganesyan, Phenomenology of fully many-body-localized systems, *Phys. Rev. B* **90**, 174202 (2014).
- [21] M. Serbyn and J. E. Moore, Spectral statistics across the many-body localization transition, *Phys. Rev. B* **93**, 041424 (2016).
- [22] R. Nandkishore and D. A. Huse, Many-Body Localization and Thermalization in Quantum Statistical Mechanics, *Annual Review of Condensed Matter Physics* **6**, 15 (2015).
- [23] D. A. Abanin, E. Altman, I. Bloch, and M. Serbyn, Colloquium: Many-body localization, thermalization, and entanglement, *Rev. Mod. Phys.* **91**, 021001 (2019).
- [24] H. Bernien, S. Schwartz, A. Keesling, H. Levine, A. Omran, H. Pichler, S. Choi, A. S. Zibrov, M. Endres, M. Greiner, *et al.*, Probing many-body dynamics on a 51-atom quantum simulator, *Nature* **551**, 579 (2017).
- [25] C. J. Turner, A. A. Michailidis, D. A. Abanin, M. Serbyn, and Z. Papić, Weak ergodicity breaking from quantum many-body scars, *Nature Physics* **14**, 745 (2018).
- [26] C. J. Turner, A. A. Michailidis, D. A. Abanin, M. Serbyn, and Z. Papić, Quantum scarred eigenstates in a Rydberg atom chain: Entanglement, breakdown of thermalization, and stability to perturbations, *Phys. Rev. B* **98**, 155134 (2018).
- [27] C.-J. Lin and O. I. Motrunich, Exact Quantum Many-Body Scar States in the Rydberg-Blockaded Atom Chain, *Phys. Rev. Lett.* **122**, 173401 (2019).
- [28] S. Moudgalya, S. Rachel, B. A. Bernevig, and N. Regnault, Exact excited states of nonintegrable models, *Phys. Rev. B* **98**, 235155 (2018).
- [29] S. Moudgalya, N. Regnault, and B. A. Bernevig, Entanglement of exact excited states of Affleck-Kennedy-Lieb-Tasaki models: Exact results, many-body scars, and violation of the strong

- eigenstate thermalization hypothesis, *Phys. Rev. B* **98**, 235156 (2018).
- [30] S. Choi, C. J. Turner, H. Pichler, W. W. Ho, A. A. Michailidis, Z. Papić, M. Serbyn, M. D. Lukin, and D. A. Abanin, Emergent SU(2) Dynamics and Perfect Quantum Many-Body Scars, *Phys. Rev. Lett.* **122**, 220603 (2019).
- [31] W. W. Ho, S. Choi, H. Pichler, and M. D. Lukin, Periodic Orbits, Entanglement, and Quantum Many-Body Scars in Constrained Models: Matrix Product State Approach, *Phys. Rev. Lett.* **122**, 040603 (2019).
- [32] N. Shiraishi, Connection between quantum-many-body scars and the Affleck–Kennedy–Lieb–Tasaki model from the viewpoint of embedded Hamiltonians, *Journal of Statistical Mechanics: Theory and Experiment* **2019**, 083103 (2019).
- [33] M. Schechter and T. Iadecola, Weak Ergodicity Breaking and Quantum Many-Body Scars in Spin-1 XY Magnets, *Phys. Rev. Lett.* **123**, 147201 (2019).
- [34] C.-J. Lin, A. Chandran, and O. I. Motrunich, Slow thermalization of exact quantum many-body scar states under perturbations, *Phys. Rev. Research* **2**, 033044 (2020).
- [35] M. Medenjak, B. Buča, and D. Jaksch, Isolated Heisenberg magnet as a quantum time crystal, *Phys. Rev. B* **102**, 041117 (2020).
- [36] D. K. Mark, C.-J. Lin, and O. I. Motrunich, Unified structure for exact towers of scar states in the Affleck-Kennedy-Lieb-Tasaki and other models, *Phys. Rev. B* **101**, 195131 (2020).
- [37] D. K. Mark and O. I. Motrunich, η -pairing states as true scars in an extended Hubbard model, *Phys. Rev. B* **102**, 075132 (2020).
- [38] S. Moudgalya, N. Regnault, and B. A. Bernevig, η -pairing in Hubbard models: From spectrum generating algebras to quantum many-body scars, *Phys. Rev. B* **102**, 085140 (2020).
- [39] N. O’Dea, F. Burnell, A. Chandran, and V. Khemani, From tunnels to towers: Quantum scars from Lie algebras and q -deformed Lie algebras, *Phys. Rev. Research* **2**, 043305 (2020).
- [40] N. Shibata, N. Yoshioka, and H. Katsura, Onsager’s Scars in Disordered Spin Chains, *Phys. Rev. Lett.* **124**, 180604 (2020).
- [41] K. Pakrouski, P. N. Pallegar, F. K. Popov, and I. R. Klebanov, Many-Body Scars as a Group Invariant Sector of Hilbert Space, *Phys. Rev. Lett.* **125**, 230602 (2020).
- [42] J. Ren, C. Liang, and C. Fang, Quasisymmetry Groups and Many-Body Scar Dynamics, *Phys. Rev. Lett.* **126**, 120604 (2021).
- [43] S. Moudgalya, B. A. Bernevig, and N. Regnault, Quantum many-body scars and Hilbert space fragmentation: a review of exact results, *Reports on Progress in Physics* **85**, 086501 (2022).
- [44] G.-X. Su, H. Sun, A. Hudomal, J.-Y. Desaulles, Z.-Y. Zhou, B. Yang, J. C. Halimeh, Z.-S. Yuan, Z. Papić, and J.-W. Pan, Observation of many-body scarring in a Bose-Hubbard quantum simulator, *Phys. Rev. Res.* **5**, 023010 (2023).
- [45] B. Buča, J. Tindall, and D. Jaksch, Non-stationary coherent quantum many-body dynamics through dissipation, *Nat. Comm.* **10**, 1730 (2019).
- [46] K. G. Wilson, Confinement of quarks, *Phys. Rev. D* **10**, 2445 (1974).
- [47] J. B. Kogut, An introduction to lattice gauge theory and spin systems, *Rev. Mod. Phys.* **51**, 659 (1979).
- [48] R. Moessner, S. L. Sondhi, and E. Fradkin, Short-ranged resonating valence bond physics, quantum dimer models, and Ising gauge theories, *Phys. Rev. B* **65**, 024504 (2001).
- [49] E. Fradkin and L. Susskind, Order and disorder in gauge systems and magnets, *Phys. Rev. D* **17**, 2637 (1978).
- [50] E. Fradkin and S. H. Shenker, Phase diagrams of lattice gauge theories with Higgs fields, *Phys. Rev. D* **19**, 3682 (1979).
- [51] E. Fradkin, *Field theories of condensed matter physics* (Cambridge University Press, Cambridge, England, 2013).
- [52] T. Byrnes and Y. Yamamoto, Simulating lattice gauge theories on a quantum computer, *Phys. Rev. A* **73**, 022328 (2006).
- [53] D. Banerjee, M. Dalmonte, M. Müller, E. Rico, P. Stebler, U.-J. Wiese, and P. Zoller, Atomic quantum simulation of dynamical gauge fields coupled to Fermionic matter: From string breaking to evolution after a quench, *Phys. Rev. Lett.* **109**, 175302 (2012).
- [54] O. Di Stefano, A. Settineri, V. Macrì, L. Garziano, R. Stassi, S. Savasta, and F. Nori, Resolution of gauge ambiguities in ultrastrong-coupling cavity quantum electrodynamics, *Nature Physics* **15**, 803 (2019).
- [55] G. Magnifico, M. Dalmonte, P. Facchi, S. Pascazio, F. V. Pepe, and E. Ercolessi, Real Time Dynamics and Confinement in the \mathbb{Z}_n Schwinger-Weyl lattice model for 1+1 QED, *Quantum* **4**, 281 (2020).
- [56] M. C. Banuls, R. Blatt, J. Catani, A. Celi, J. I. Cirac, M. Dalmonte, L. Fallani, K. Jansen, M. Lewenstein, S. Montangero, *et al.*, Simulating lattice gauge theories within quantum technologies, *The European physical journal D* **74**, 1 (2020).
- [57] A. Settineri, O. Di Stefano, D. Zueco, S. Hughes, S. Savasta, and F. Nori, Gauge freedom, quantum measurements, and time-dependent interactions in cavity QED, *Phys. Rev. Res.* **3**, 023079 (2021).
- [58] S. Savasta, O. Di Stefano, A. Settineri, D. Zueco, S. Hughes, and F. Nori, Gauge principle and gauge invariance in two-level systems, *Phys. Rev. A* **103**, 053703 (2021).
- [59] E. Rinaldi, X. Han, M. Hassan, Y. Feng, F. Nori, M. McGuigan, and M. Hanada, Matrix-Model Simulations Using Quantum Computing, Deep Learning, and Lattice Monte Carlo, *PRX Quantum* **3**, 010324 (2022).
- [60] J. C. Halimeh, L. Barbiero, P. Hauke, F. Grusdt, and A. Bohrdt, Robust quantum many-body scars in lattice gauge theories, *Quantum* **7**, 1004 (2023).
- [61] J.-Y. Desaulles, D. Banerjee, A. Hudomal, Z. Papić, A. Sen, and J. C. Halimeh, Weak ergodicity breaking in the Schwinger model, *Phys. Rev. B* **107**, L201105 (2023).
- [62] J.-Y. Desaulles, A. Hudomal, D. Banerjee, A. Sen, Z. Papić, and J. C. Halimeh, Prominent quantum many-body scars in a truncated Schwinger model, *Phys. Rev. B* **107**, 205112 (2023).
- [63] A. J. A. James, R. M. Konik, and N. J. Robinson, Nonthermal States Arising from Confinement in One and Two Dimensions, *Phys. Rev. Lett.* **122**, 130603 (2019).
- [64] N. J. Robinson, A. J. A. James, and R. M. Konik, Signatures of rare states and thermalization in a theory with confinement, *Phys. Rev. B* **99**, 195108 (2019).
- [65] F. M. Surace, P. P. Mazza, G. Giudici, A. Lerose, A. Gambassi, and M. Dalmonte, Lattice Gauge Theories and String Dynamics in Rydberg Atom Quantum Simulators, *Phys. Rev. X* **10**, 021041 (2020).
- [66] T. Iadecola and M. Schechter, Quantum many-body scar states with emergent kinetic constraints and finite-entanglement revivals, *Phys. Rev. B* **101**, 024306 (2020).
- [67] Z.-C. Yang, F. Liu, A. V. Gorshkov, and T. Iadecola, Hilbert-Space Fragmentation from Strict Confinement, *Phys. Rev. Lett.* **124**, 207602 (2020).
- [68] D. Banerjee and A. Sen, Quantum Scars from Zero Modes in an Abelian Lattice Gauge Theory on Ladders, *Phys. Rev. Lett.* **126**, 220601 (2021).
- [69] A. S. Aramthottil, U. Bhattacharya, D. González-Cuadra, M. Lewenstein, L. Barbiero, and J. Zakrzewski, Scar states in deconfined \mathbb{Z}_2 lattice gauge theories, *Phys. Rev. B* **106**, L041101 (2022).
- [70] L. Pan and H. Zhai, Composite spin approach to the block-

- ade effect in Rydberg atom arrays, *Phys. Rev. Res.* **4**, L032037 (2022).
- [71] A. Chandran, T. Iadecola, V. Khemani, and R. Moessner, Quantum Many-Body Scars: A Quasiparticle Perspective, *Annual Review of Condensed Matter Physics* **14**, 443 (2023).
- [72] M. Kormos, M. Collura, G. Takacs, and P. Calabrese, Real-time confinement following a quantum quench to a non-integrable model, *Nat. Phys.* **13**, 246 (2017).
- [73] S. Birnkammer, A. Bastianello, and M. Knap, Prethermalization in one-dimensional quantum many-body systems with confinement, *Nature Communications* **13**, 7663 (2022).
- [74] L. Barbiero, C. Schweizer, M. Aidelsburger, E. Demler, N. Goldman, and F. Grusdt, Coupling ultracold matter to dynamical gauge fields in optical lattices: From flux attachment to Z_2 lattice gauge theories, *Sci. Adv.* **5**, eaav7444 (2019).
- [75] C. Schweizer, F. Grusdt, M. Berngruber, L. Barbiero, E. Demler, N. Goldman, I. Bloch, and M. Aidelsburger, Floquet approach to $Z(2)$ lattice gauge theories with ultracold atoms in optical lattices, *Nat. Phys.* **15**, 1168 (2019).
- [76] F. Goerg, K. Sandholzer, J. Minguzzi, R. Desbuquois, M. Messer, and T. Esslinger, Realization of density-dependent Peierls phases to engineer quantized gauge fields coupled to ultracold matter, *Nat. Phys.* **15**, 1161 (2019).
- [77] Z.-Y. Ge, R.-Z. Huang, Z.-Y. Meng, and H. Fan, Quantum simulation of lattice gauge theories on superconducting circuits: Quantum phase transition and quench dynamics, *Chin. Phys. B* **31**, 020304 (2021).
- [78] Z. Wang, Z.-Y. Ge, Z. Xiang, X. Song, R.-Z. Huang, P. Song, X.-Y. Guo, L. Su, K. Xu, D. Zheng, and H. Fan, Observation of emergent Z_2 gauge invariance in a superconducting circuit, *Phys. Rev. Research* **4**, L022060 (2022).
- [79] J. Mildenerberger, W. Mruczkiewicz, J. C. Halimeh, Z. Jiang, and P. Hauke, Probing confinement in a Z_2 lattice gauge theory on a quantum computer, *arXiv:2203.08905*.
- [80] R. Irmejs, M. C. Banuls, and J. I. Cirac, Quantum Simulation of Z_2 Lattice Gauge theory with minimal requirements, *arXiv:2206.08909*.
- [81] Z.-Y. Ge and F. Nori, Confinement-induced enhancement of superconductivity in a spin- $\frac{1}{2}$ fermion chain coupled to a Z_2 lattice gauge field, *Phys. Rev. B* **107**, 125141 (2023).
- [82] M. Kebrić, L. Barbiero, C. Reinmoser, U. Schollwöck, and F. Grusdt, Confinement and Mott transitions of dynamical charges in one-dimensional lattice gauge theories, *Phys. Rev. Lett.* **127**, 167203 (2021).
- [83] D. N. Page, Average entropy of a subsystem, *Phys. Rev. Lett.* **71**, 1291 (1993).
- [84] See Supplemental Material.
- [85] Due to the chiral symmetry in the Hamiltonian when neglecting \hat{H}_μ , i.e., $\hat{P}\hat{H}\hat{P}^\dagger = -\hat{H}$ with $\hat{P} := \prod_j \hat{\tau}_{j+\frac{1}{2}}^y$, a scar state with total string length $l \geq L/2$ is equivalent to a scar state with total string length $(L-l)$. In addition, the eigenenergy of a scar state with $l = L/2$ is zero (the central part of the spectrum), corresponding to an infinite-temperature system. Therefore, we only need to consider the total string length $l \leq L/2$, and the large total string length means that l is $\approx L/2$.
- [86] X. Zhang, W. Jiang, J. Deng, K. Wang, J. Chen, P. Zhang, W. Ren, H. Dong, S. Xu, Y. Gao, *et al.*, Digital quantum simulation of Floquet symmetry-protected topological phases, *Nature* **607**, 468 (2022).
- [87] D. J. Gross and F. Wilczek, Ultraviolet Behavior of Non-Abelian Gauge Theories, *Phys. Rev. Lett.* **30**, 1343 (1973).
- [88] H. D. Politzer, Reliable Perturbative Results for Strong Interactions?, *Phys. Rev. Lett.* **30**, 1346 (1973).
- [89] T. Iadecola, M. Schechter, and S. Xu, Quantum many-body scars from magnon condensation, *Phys. Rev. B* **100**, 184312 (2019).
- [90] E. Dagotto, E. Fradkin, and A. Moreo, SU(2) gauge invariance and order parameters in strongly coupled electronic systems, *Phys. Rev. B* **38**, 2926 (1988).

Supplemental Material: Nonmesonic Quantum Many-Body Scars in a 1D Lattice Gauge Theory

I. Quantum Many-Body Scars

A. Proof of $\hat{H}_K |\Psi_{n,l}\rangle = 0$

In the main text, we show that the wave function

$$|\Psi_{n,l}\rangle = \mathcal{N}_{n,l} \sum P_{\{\mathcal{S}_{k_j, \ell_j}\}_n^l} |\{\mathcal{S}_{k_j, \ell_j}\}_n^l\rangle, \quad (\text{S1})$$

is an exact eigenstate of \hat{H} . Here we present details for proving this result. It is not difficult to find that $\hat{H}_E |\Psi_{n,l}\rangle = h(2l - L) |\Psi_{n,l}\rangle$, so we only need to prove $\hat{H}_K |\Psi_{n,l}\rangle = 0$. Since the action of \hat{H}_K is increasing or reducing the total string length by one, while keeping n invariant, we have

$$\hat{H}_K |\Psi_{n,l}\rangle = \sum c_{\{\mathcal{S}_{k'_j, \ell'_j}\}_n^{l-1}} |\{\mathcal{S}_{k'_j, \ell'_j}\}_n^{l-1}\rangle + \sum c_{\{\mathcal{S}_{k'_j, \ell'_j}\}_n^{l+1}} |\{\mathcal{S}_{k'_j, \ell'_j}\}_n^{l+1}\rangle. \quad (\text{S2})$$

Here, the factors have forms

$$\begin{aligned} c_{\{\mathcal{S}_{k'_j, \ell'_j}\}_n^{l-1}} &= \mathcal{N}_{n,l} \sum [(1 - \delta_{k'_1 + \ell'_1 + 1, k'_2}) (P_{\mathcal{S}_{k'_1, \ell'_1 + 1}, \mathcal{S}_{k'_2, \ell'_2} \dots} + P_{\mathcal{S}_{k'_1, \ell'_1}, \mathcal{S}_{k'_2 - 1, \ell'_2 + 1} \dots}) \\ &\quad + (1 - \delta_{k'_2 + \ell'_2 + 1, k'_3}) (P_{\dots, \mathcal{S}_{k'_2, \ell'_2 + 1}, \mathcal{S}_{k'_3, \ell'_3} \dots} + P_{\dots, \mathcal{S}_{k'_2, \ell'_2}, \mathcal{S}_{k'_3 - 1, \ell'_3 + 1} \dots}) + \dots \\ c_{\{\mathcal{S}_{k'_j, \ell'_j}\}_n^{l+1}} &= \mathcal{N}_{n,l} \sum [(1 - \delta_{\ell'_1, 1}) (P_{\mathcal{S}_{k'_1 - 1, \ell'_1 - 1}, \mathcal{S}_{k'_2, \ell'_2} \dots} + P_{\mathcal{S}_{k'_1, \ell'_1 - 1}, \mathcal{S}_{k'_2, \ell'_2} \dots}) \\ &\quad + (1 - \delta_{\ell'_2, 1}) (P_{\dots, \mathcal{S}_{k'_2 - 1, \ell'_2 - 1}, \mathcal{S}_{k'_3, \ell'_3} \dots} + P_{\dots, \mathcal{S}_{k'_2, \ell'_2 - 1}, \mathcal{S}_{k'_3, \ell'_3} \dots}) + \dots \end{aligned} \quad (\text{S3})$$

Since the parity satisfies $P_{\mathcal{S}_{k'_1, \ell'_1}, \dots, \mathcal{S}_{k'_j, \ell'_j}, \dots, \mathcal{S}_{k'_n, \ell'_n}} = \exp(i\pi \sum_j k'_j)$, we have

$$\begin{aligned} P_{\dots, \mathcal{S}_{k'_{j-1}, \ell'_{j-1}}, \mathcal{S}_{k'_j, \ell'_j + 1}, \mathcal{S}_{k'_{j+1}, \ell'_{j+1}} \dots} &= -P_{\dots, \mathcal{S}_{k'_{j-1}, \ell'_{j-1}}, \mathcal{S}_{k'_j, \ell'_j}, \mathcal{S}_{k'_{j+1} - 1, \ell'_{j+1} + 1} \dots} \\ P_{\dots, \mathcal{S}_{k'_{j-1}, \ell'_{j-1}}, \mathcal{S}_{k'_j - 1, \ell'_j - 1}, \mathcal{S}_{k'_{j+1}, \ell'_{j+1}} \dots} &= -P_{\dots, \mathcal{S}_{k'_{j-1}, \ell'_{j-1}}, \mathcal{S}_{k'_j, \ell'_j - 1}, \mathcal{S}_{k'_{j+1}, \ell'_{j+1}} \dots} \end{aligned} \quad (\text{S4})$$

Therefore, $c_{\{\mathcal{S}_{k'_j, \ell'_j}\}_n^{l-1}} = c_{\{\mathcal{S}_{k'_j, \ell'_j}\}_n^{l+1}} = 0$, i.e., $\hat{H}_K |\Psi_{n,l}\rangle = 0$.

B. Proof of $|\Psi_{n,n+m}\rangle = \mathcal{D}_{n,m} \hat{L}_m^\dagger |\Psi_{n,n+m-1}\rangle$

Next we show the detail of proving Eq. (8) in the main text, i.e.,

$$|\Psi_{n,n+m}\rangle = \mathcal{D}_{n,m} \hat{L}_m^\dagger |\Psi_{n,n+m-1}\rangle, \quad (\text{S5})$$

where $\mathcal{D}_{n,m}$ is a normalization factor, and

$$\hat{L}_m^\dagger = \sum_j \left(\sum_{k \leq m} \prod_{\ell \leq k} \hat{\mathcal{P}}_{j+\frac{1}{2}-\ell}^- \right) \hat{\sigma}_j^- \hat{\tau}_{j+\frac{1}{2}}^M \hat{\sigma}_{j+1}^+ \quad (\text{S6})$$

It is not difficult to demonstrate

$$\left(\sum_{k \leq m} \prod_{\ell \leq k} \hat{\mathcal{P}}_{j+\frac{1}{2}-\ell}^- \right) \hat{\sigma}_j^- \hat{\tau}_{j+\frac{1}{2}}^M \hat{\sigma}_{j+1}^+ |\mathcal{S}_{k,\ell}\rangle = \begin{cases} \ell \delta_{j,k+\ell} |\mathcal{S}_{k,\ell+1}\rangle & \ell \leq m \\ m \delta_{j,k+\ell} |\mathcal{S}_{k,\ell+1}\rangle & \ell > m. \end{cases} \quad (\text{S7})$$

Thus, the action of \hat{L}_m^\dagger is increasing the total string length of a basis without changing the parity and string number. Therefore,

$$\hat{L}_m^\dagger |\Psi_{n,n+m-1}\rangle = \sum \alpha_{\{\mathcal{S}_{k'_j, \ell'_j}\}_n^{n+m}} |\{\mathcal{S}_{k'_j, \ell'_j}\}_n^{n+m}\rangle. \quad (\text{S8})$$

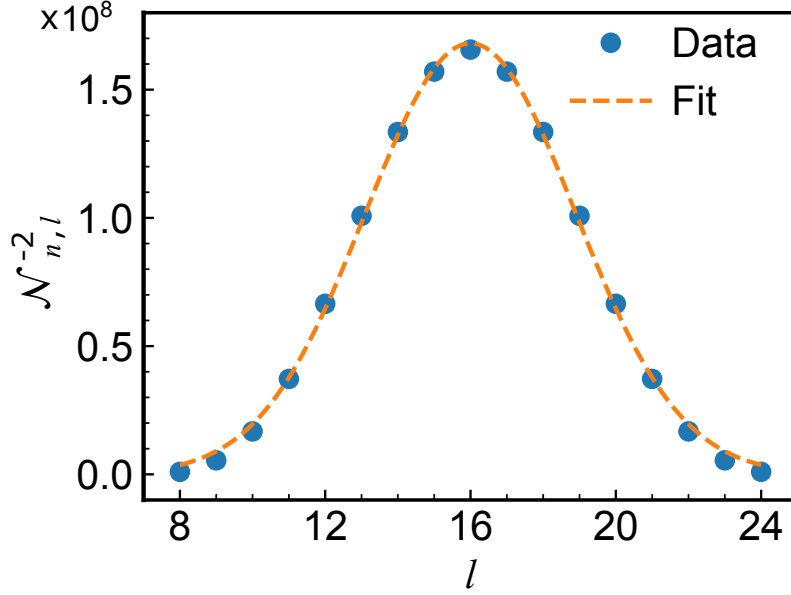


FIG. S1. Distribution of $\mathcal{N}_{n,l}^{-2}$ for $L = 32$ and $n = 8$ (half filling). The orange dashed curve is a Gaussian fit.

For the wave function $|\Psi_{n,n+m-1}\rangle = \mathcal{N}_{n,n+m-1} \sum P_{\{\mathcal{S}_{k_j, \ell_j}\}_n^{n+m-1}} |\{\mathcal{S}_{k_j, \ell_j}\}_n^{n+m-1}\rangle$, the length of each string satisfies $\ell_j \leq m$. Hence, the factor has the form

$$\alpha_{\{\mathcal{S}_{k'_j, \ell'_j}\}_n^{n+m}} = \mathcal{N}_{n,n+m-1} P_{\{\mathcal{S}_{k'_j, \ell'_j}\}_n^{n+m}} [(1 - \delta_{\ell'_1, 1})(\ell'_1 - 1) + (1 - \delta_{\ell'_2, 1})(\ell'_2 - 1) + \dots + (1 - \delta_{\ell'_n, 1})(\ell'_n - 1)]. \quad (\text{S9})$$

If $\ell'_j = 1$, then $(1 - \delta_{\ell'_j, 1})(\ell'_j - 1) = (\ell'_j - 1) = 0$, and if $\ell'_j \neq 1$, then $(1 - \delta_{\ell'_j, 1})(\ell'_j - 1) = (\ell'_j - 1)$. Thus

$$\alpha_{\{\mathcal{S}_{k'_j, \ell'_j}\}_n^{n+m}} = \mathcal{N}_{n,n+m-1} P_{\{\mathcal{S}_{k'_j, \ell'_j}\}_n^{n+m}} \sum_{j=1}^n (\ell'_j - 1) = \mathcal{N}_{n,n+m-1} P_{\{\mathcal{S}_{k'_j, \ell'_j}\}_n^{n+m}} (m - 1). \quad (\text{S10})$$

Therefore, we have

$$\hat{L}_m^\dagger |\Psi_{n,n+m-1}\rangle = (m - 1) \mathcal{N}_{n,n+m-1} \sum P_{\{\mathcal{S}_{k'_j, \ell'_j}\}_n^{n+m}} |\{\mathcal{S}_{k'_j, \ell'_j}\}_n^{n+m}\rangle = \frac{(m - 1) \mathcal{N}_{n,n+m-1}}{\mathcal{N}_{n,n+m}} |\Psi_{n,n+m}\rangle. \quad (\text{S11})$$

That is, Eq. (8) is proved, and the normalization factor satisfies

$$\mathcal{D}_{n,m} = \frac{\mathcal{N}_{n,n+m}}{(m - 1) \mathcal{N}_{n,n+m-1}}. \quad (\text{S12})$$

II. Initial state

Here we discuss the initial state $|\psi_2\rangle$ in Eq. (10b) of the main text, where it reads

$$|\psi_2\rangle = \frac{1}{2^{L/2}} \sum_{n,l} \sum_{\{k_j, \ell_j\}} P_{\{\mathcal{S}_{k_j, \ell_j}\}_n^l} |\{\mathcal{S}_{k_j, \ell_j}\}_n^l\rangle = \sum_{n,l} \beta_{n,l} |\Psi_{n,l}\rangle. \quad (\text{S13})$$

The amplitude $\beta_{n,l}$ satisfies $\beta_{n,l} = 1/\mathcal{N}_{n,l} 2^{L/2}$, where $\mathcal{N}_{n,l}$ is the normalization factor defined in Eq. (6) of the main text. In addition, $\mathcal{N}_{n,l}^{-2}$ is the number of string bases for the scar state $|\Psi_{n,l}\rangle$, and it can be obtained as

$$\mathcal{N}_{n,l}^{-2} = \binom{l-1}{n-1} \left[\binom{L-l-1}{n} + 2 \binom{L-l-1}{n-1} \right] + \binom{L-l-1}{n-1} \binom{l-1}{n}, \quad (\text{S14})$$

where $\binom{\cdot}{\cdot}$ is the combinatorial number. In Fig. S1, we show the result of $\mathcal{N}_{n,l}^{-2}$ versus l for $L = 32$ and $n = 8$ (half filling). We can find that $\mathcal{N}_{n,l}^{-2}$ nearly satisfies a Gaussian distribution with the symmetric point at $l = L/2$. Therefore, for the initial state $|\psi_2\rangle$ the nonmesonic scar states dominate.